Surface vacancy mediated pinning of the magnetization in γ-Fe$_2$O$_3$ nanoparticles: A micromagnetic simulation study

Bassel Alkadour,[1] J. I. Mercer,[2] J. P. Whitehead,[1] J. van Lierop,[3] and B. W. Southern[3]

[1]*Department of Physics and Physical Oceanography, Memorial University, St. John's, Newfoundland and Labrador, Canada A1B 3X7*
[2]*Department of Computer Science, Memorial University, St. John's, Newfoundland and Labrador, Canada A1B 3X5*
[3]*Department of Physics and Astronomy, University of Manitoba, Winnipeg, Manitoba, Canada R3T 2N2*

Results from finite temperature sLLG simulations of an atomistic core-shell model of γ-Fe$_2$O$_3$ nanoparticles are presented. Radial surface anisotropy gives rise to a surface magnetization with a Néel-like domain wall separating the magnetic poles. It is shown that the pinning of the domain wall by the oxygen anion sites plays an important role in low temperature relaxation processes.

The sensitivity of nanoparticle properties to small changes in composition and morphology has motivated the research and development of increasingly complex materials. Indeed, the impact of nanoparticle research is substantial; advances in several areas such as nanomedicine, energy storage, and environmental remediation [1] have benefited from modern advances in preparation and characterization techniques. Of particular interest is the "single-domain" magnetic nanoparticle that offers a means of attaining properties not accessible in bulk systems, for example, the observation of exchange-bias [2] and catalytic [3] properties. Such magnetic nanoparticles (characteristic dimensions in the range of 1 up to ∼50 nm, depending on the crystal structure) exhibit properties that are not possible in the bulk because of their large surface-to-volume ratio. A noncollinear surface magnetization is the archetypical feature whose precise structure will depend on the form and strength of the surface anisotropy and exchange interactions between atoms.

Maghemite-based materials are prime candidates for understanding in detail the impact of surface spin magnetism and its application due to the variability of the magnetism that can be achieved by cation substitution into the structure. Maghemite (γ-Fe$_2$O$_3$) adopts the spinel structure that is based on a face-centered-cubic lattice of oxygen anions. Each unit cell contains 32 O^{2-} ions, and 16 of 32 available octahedral and 8 of 64 available tetrahedral interstitial sites can be occupied by various cations. γ-Fe$_2$O$_3$ (as magnetite, Fe$_3$O$_4$) is an inverse spinel of the form $(Y)[XY]$O$_4$, where X is a divalent (Fe^{2+}) ion and Y is a trivalent (Fe^{3+}) ion that occupies the tetrahedral () and octahedral [] A and B sites. Fe$_3$O$_4$ and the other ferrites are fully occupied inverse spinels; γ-Fe$_2$O$_3$ contains no divalent ions. To maintain charge balance, it has octahedral site vacancies. Thus, γ-Fe$_2$O$_3$ can be described as (Fe^{3+})$_A$[Fe$^{3+}_{5/3}$□$_{1/3}$]$_B$O$_4$, where each unit cell contains 32 O^{2-} ions, 8 tetrahedral (A-site) Fe^{3+} ions, 40/3 octahedral (B-site) Fe^{3+} ions, and 8/3 vacant (□) octahedral sites. The versatility of the structure arises from the stability available over a wide range of stoichiometry, and in nanoparticles, the surface octahedral site vacancies [4] enable surface spin disorder through broken coordination of neighboring ions, resulting in noncollinear surface magnetizaton [5]. The nature of γ-Fe$_2$O$_3$'s surface magnetization determines, in large part, the overall magnetization and anisotropy of a nanoparticle [6,7], the effect of which can be observed in the magnetization's field and temperature

dependence (hysteresis loops) [8,9], ac and dc susceptibility measurements [10], and the blocking temperature [11], T_B.

In this Rapid Communication we present results from a series of simulations on ensembles of spherical γ-Fe$_2$O$_3$ nanoparticles using the finite temperature stochastic Landau-Lifshitz-Gilbert (sLLG) equation based on an atomistic core spin-surface spin (shell) model [12]. Such atomistic models provide a more detailed description of magnetic nanoparticles than those composed of a system of coupled superspins [13–16]. The simulations show that the competition between a radial surface anisotropy and an antiferromagnetic exchange gives rise to a ferrimagnetic surface magnetization that is characterized by a Néel-like domain wall located at the magnetic equator separating the magnetic north and south poles of the nanoparticle at low temperature. It is also shown that the presence of oxygen anions in γ-Fe$_2$O$_3$ results in a surface pinning mechanism that plays a critical role in determining the nonequilibrium magnetic response of spherical γ-Fe$_2$O$_3$ 7 nanoparticles at low temperatures. A result that is perhaps counterintuitive given that such particles are generally considered single domain.

The core-shell model is based on the observation that the surface spins in γ-Fe$_2$O$_3$ nanoparticles are observed to order at around $T_{sf} \approx 30$ K, a much lower temperature than the core atoms which will be close to the estimated transition temperature for bulk γ-Fe$_2$O$_3$ ($T_c \approx 850$ K) [17], with a surface magnetization that is noncollinear. This is attributed to the change in the environment of the Fe^{3+} ions located close to the nanoparticle surface that results in a weaker exchange interaction and a radial anisotropy. In the absence of a precise description of the variation in the exchange and radial anisotropy at the surface, the core-shell model separates the Fe ion locations between the core and surface sites [11,12] in which those sites for which $r < D_c/2$ are designated core sites and $D_c/2 < r < D/2$ are designated surface sites, where D_c denotes the core diameter and r the distance of the site from the center of the sphere. The energy for a given spin configuration is given by

$$E = -\sum_{\langle ij \rangle} J_{ij}\hat{S}_i \cdot \hat{S}_j - \sum_{i \in \text{surface}} K_s(\hat{S}_i \cdot \hat{n}_i)^2 - \mu_0 \sum_i \vec{H} \cdot \vec{\mu}_i,$$

where $\hat{S}_i = \vec{\mu}_i/\mu_S$ denotes the normalized magnetic moment vector $\vec{\mu}_i$ of the Fe^{3+} ion on the ith site, $\mu_S = g_J S \mu_B$ ($g_J S =$

5), J_{ij} is the exchange interaction which depends on whether the i and j refer to A or B, surface, or core sites, the sum $\sum_{\langle ij \rangle}$ is over all nearest neighbor pairs, and K_s denotes the surface anisotropy with its axis $\hat{n}_i$ directed radially outwards. It is assumed that the anisotropy at the core sites is equal to that of bulk γ-Fe$_2$O$_3$, which is relatively small [18,19], and is therefore set to zero in our simulations.

In this Rapid Communication simulation results are presented for spherical γ-Fe$_2$O$_3$ nanoparticles with a diameter $D = 5$ nm with a core diameter $D_c = 3.67$ nm resulting in a Fe^{3+} ion core-to-surface volume ratio of 40%. The values for the core-core exchange are $J_{cc}^{ab}/(g_J S)^2 k_B = -56.2$ K, $J_{cc}^{aa}/(g_J S)^2 k_B = -42.0$ K, and $J_{cc}^{bb}/(g_J S)^2 k_B = -17.2$ K, where the superscripts a and b distinguish between A and B sites and subscript c denotes the core sites. These values are consistent with experimental values for bulk γ-Fe$_2$O$_3$ [8,17]. Comparing the temperature T_{sf} at which the surface spins start to order with the estimated transition temperature for bulk γ-Fe$_2$O$_3$ suggests that the surface exchange is approximately a factor 40 smaller than the corresponding interactions between the core sites (i.e., $J_{sc}^{aa} = J_{ss}^{aa} = 0.025 J_{cc}^{aa}$). While reasonable estimates of both core diameter and the surface exchange of the γ-Fe$_2$O$_3$ nanoparticles may be obtained from the magnetization curves, the determination of surface anisotropy constant K_s is somewhat more elusive. Results are therefore presented for two ensembles, each consisting of 1000 nanoparticles, with $K_s/k_B = 5.0$ K and $K_s/k_B = 10.0$ K (values chosen to demonstrate the effect of the surface anisotropy), which we refer to as the K5 and the K10 ensembles, respectively. A comparison of these results from these two ensembles provides some insight into the role the surface anisotropy plays in determining the characteristic properties of γ-Fe$_2$O$_3$ nanoparticles.

The sLLG equation of motion for the spin magnetic moment is given by [20]

$$\frac{d\hat{S}_i}{dt} = -\gamma \mu_0 \left[\hat{S}_i \times \vec{H}_{\text{eff}} + \alpha \, \hat{S}_i \times \left(\hat{S}_i \times \vec{H}_{\text{eff}}^i \right) \right],$$

where γ is the electron gyromagnetic ratio and α the damping constant. The effective field $\mu_0 \vec{H}_{\text{eff}}^i = -\partial E / \partial \vec{S}_i + \mu_0 \vec{H}_{\text{th}}^i$ and includes the thermal field $H_{\text{th}}^i = \sqrt{2\alpha K_B T / \gamma \mu_S \Delta t} \, W_t$, where V is the volume, Δt is the time step, and W_t is a stochastic variable that describes a Wiener process $\langle W_t W_{t'} \rangle = \delta(t - t')$. For convenience we define the time unit $t_u = 1$ T$/\gamma = 5.68 \times 10^{-12}$ s. Since the focus of the present work is on the relaxation process of the nanoparticles to a minimum in the free energy rather than their dynamical properties, a damping factor of $\alpha = 0.5$ used. The time step used to integrate the sLLG equation is $\Delta t = 2.0 \times 10^{-4} t_u$.

To demonstrate that the model described above is consistent with the observed magnetic behavior of γ-Fe$_2$O$_3$ nanoparticles, simulation results for the equilibrium magnetization of the individual nanoparticles as a function of temperature for both the K5 and K10 ensembles are shown in Fig. 1. The order parameters M_{np}, M_{cr}, and M_{sf} plotted in Fig. 1 denote the average magnitude of the magnetization of the individual nanoparticles, the core spins, and the surface spins, respectively. In all cases the order parameters are normalized to unity at saturation, where the saturated ferrimagnetic state
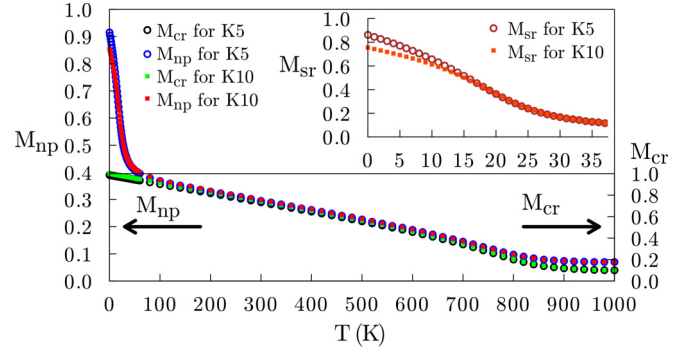
FIG. 1. The average magnitude of the core magnetization M_{cr}, the surface magnetization M_{sr}, and the nanoparticle magnetization M_{np} plotted as functions of temperature for the K5 and the K10 ensembles (zero field).

of a nanoparticle is defined as one in which the B-site spins are completely parallel to each other and antiparallel to the A-site spins.

The data show that the core spins order at a temperature $T_{cr} \approx 850$ K, in agreement with bulk γ-Fe$_2$O$_3$ [17], while the surface spins order at a much lower temperature, $T_{sf} \approx 30$ K. We also note that the surface spins in both ensembles do not fully saturate at $T = 0$ K due to the competition between the radial surface anisotropy and the exchange interactions. These results are consistent with the earlier Monte Carlo (MC) simulations [12] and experimental results [21]. It is also worth noting that the inset in Fig. 1 shows that while the surface spins begin to order at $T_s \sim 30$ K for both the K5 and K10 ensembles, it is only for $T < 12$ K that the surface magnetization for the two ensembles shows any discernible difference with $M_{sr}(\text{K10}) < M_{sr}(\text{K5})$.

To determine T_B of the nanoparticles, both the K5 and K10 ensembles were equilibrated at an initial temperature of 50 K before being cooled to 0 K [zero field cooled (ZFC)] at a rate of 0.1 K$/t_u$. A constant external magnetic field was then applied along the z axis with $\mu_B \mu_0 H_z / k_B = 0.08$ K, giving rise to a small increase in M_z, the net magnetization of the ensemble. Both ensembles were then heated to a temperature of 50 K and cooled again (in the presence of the applied field) to zero at a constant rate of 0.1 K$/t_u$. The net magnetizations M_z of both the K5 and K10 ensembles are shown in Fig. 2. The magnetization data show a significant divergence between the heating and cooling curves below the blocking temperatures $T_B \approx 12$ and 20 K for the K5 ensemble and K10 ensemble, respectively. The reason for this nonergodic behavior below T_B is due to the time required for the ensembles to equilibrate on heating being much longer than the characteristic time scale associated with the heating rate. Although not shown, simulations on ZFC K10 ensembles for different cooling and heating rates (0.1 K$/t_u$ vs 0.05 K$/t_u$) also present a small, but nevertheless discernible, difference in the blocking temperature, with the more rapid heating/cooling rate giving a slightly higher value of T_B. We note that the dependence of T_B on the anisotropy and the heating rate is qualitatively consistent with an Arrhenius-Néel process.

While the results from the simulations are qualitatively consistent with experimental observation, the cooling and
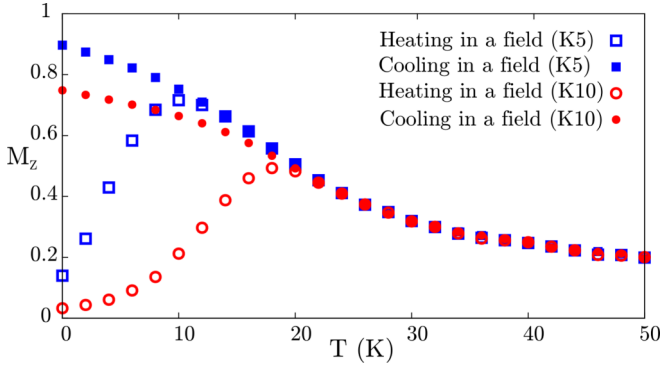
FIG. 2. Data showing the magnetization of the zero field cooled ensembles K10 and K5 during the heating and then the cooling processes under an applied field of $\mu_0 H_z/\mu_B k_B = 0.08$ K (0.12 T), where the heating and cooling rate is 0.1 K/t_u (1.76×10^{11} K/s).

heating rates and applied fields used in the simulations performed here are of the order of 0.1 K/$t_u \simeq 1.8 \times 10^{11}$ K/s and $\mu_0 H_z = 0.4$ K $\times k_B/\mu_B \approx 120$ mT, respectively. Typically, the heating and cooling rates used in the experiments are of the order of 1 K/min and the applied fields are of the order of 10 mT [21]. This difference between experiment and simulation is an inherent limitation of the sLLG approach which, in the case of these simulations, is limited to time steps of the order of $\Delta t \approx 10^{-3}$–10^{-5} ns, and hence a quantitative comparison involving experimental time scales is currently not feasible using sLLG.

To obtain a quantitative understanding of the spin configuration at the atomistic level, the radial and tangential components, $S_r = \vec{S} \cdot \hat{e}_r$, $S_\theta = \vec{S} \cdot \hat{e}_\theta$, and $S_\phi = \vec{S} \cdot \hat{e}_\phi$, of the surface spins for a single nanoparticle in the ZFC K10 ensemble at $T = 0$ are plotted in Fig. 3 as a function of $\cos\theta$ (the A site's spins are rotated 180° for convenience), with the spherical coordinates θ and ϕ defined relative to the magnetization axis of the nanoparticle. While the data show a considerable degree of scatter, it is clear that spins to the right of the vertical axis ($\cos\theta > 0$) point radially outwards,
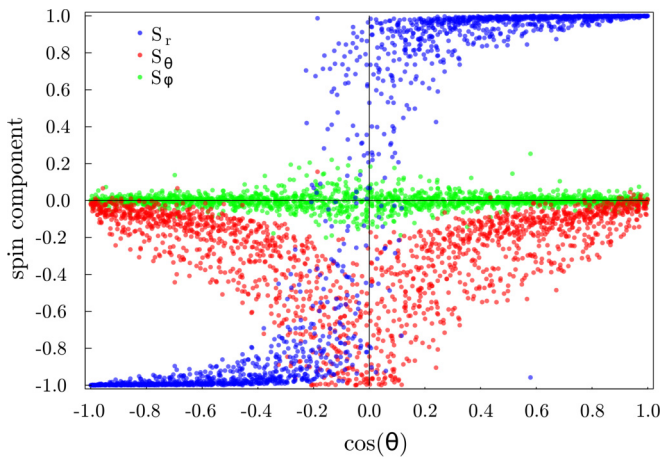
FIG. 3. A plot of the radial and tangential components of the surface spins for a single nanoparticle from a zero field cooled K10 ensemble at $T = 0$ K as a function of $\cos\theta$.
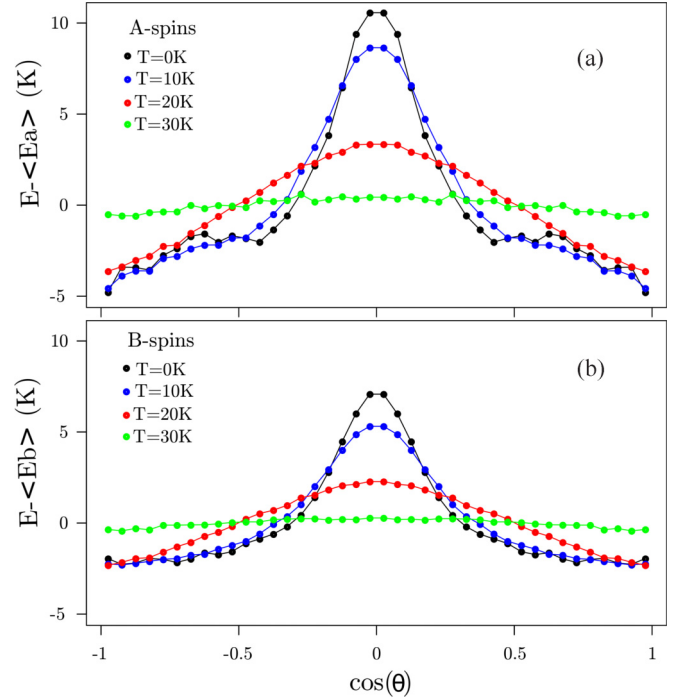
FIG. 4. The variation in average energy per spin as a function of polar angle relative to its mean value for nanoparticles belonging to the K10 ensemble at different temperatures for (a) the A sites and (b) the B sites. The ensembles have been cooled at a rate of 0.1 K/t_u under zero external field.

while the spins to the left of the vertical axis ($\cos\theta < 0$) are pointing radially inwards. Thus, the surface spins may be separated into two distinct domains corresponding to the north and south hemispheres, separated by a domain wall, located at the equator, in which the spins lie predominantly in the $\hat{e}_r \times \hat{e}_\theta$ plane; the domain wall is a Néel-type configuration.

The extent of the domain wall can also be inferred from the variation in the ensemble averaged energy per surface spin, plotted in Fig. 4, as function of $\cos\theta$ relative to its mean value for $T = 0$, 10, 20, and 30 K. There is a maximum in the energy per surface spin at the equator due to the increased exchange energy and since, at the center of the domain wall, the spins are aligned on average perpendicular to the anisotropy axis. The energy distribution becomes more homogeneous with increasing temperature due to the increased disorder of the surface spins.

Somewhat surprising are the results presented in Fig. 5 in which the angular distribution of the surface vacancies with respect to the magnetic axis of the individual nanoparticles are plotted. The vacancies appear to be clustered about the equator at low temperatures ($T < 30$ K). This would seem to be at odds with the random nature of the vacancy distribution on the B sites and that the location of vacancies (i.e., the oxygen ions) are fixed.

To understand the vacancy distribution in Fig. 5 we first note that while the vacancies are distributed randomly on the B sites, this does not imply that they are uniformly distributed among the surface sites due to the combined effects of statistical variance and the crystalline structure of γ-Fe$_2$O$_3$. In addition, while the locations of the vacancies are fixed,
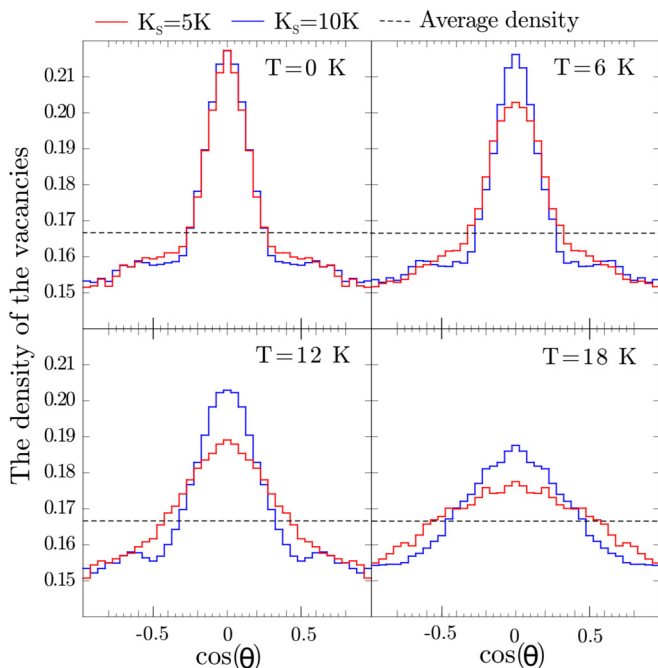
FIG. 5. The polar distribution of surface vacancies for the ensembles K10 and K5 as a function of $\cos\theta$ at different temperatures. The ensembles have been cooled with rate of 0.1 K/t_u under zero external field.

FIG. 6. The energy landscape for a nanoparticle selected at random from the K10 enemble. Each point on the surface of the sphere represents the energy associated with the alignment of the magnetic moment. The energy is calculated using a mean field approximation based on the distribution of surface vacancies and the average angular distribution of the energy per spins at $T = 0$ shown in Fig. 4. The energy scale associated with the color map shown on the right is given in K.

their angular distribution is determined by the orientation of the magnetization axis of the individual nanoparticles. The magnetization axis of the individual nanoparticles is not fixed, and will move in response to the applied magnetic field and the thermal fluctuations. At low temperature the magnetic axis of the individual nanoparticles will align to minimize the energy of spins and hence align the magnetization axis to maximize the number of vacancies at the equator as the "equatorial spins" have the highest energy. The effect of the surface vacancies is therefore to pin to the equatorial domain wall, giving rise to low energy, metastable spin configurations resulting in the concentration of vacancies shown in Fig. 5.

To illustrate the effect of the pinning (based on a mean field approximation), the variation in the energy of an individual nanoparticle due to the change in the polar distribution of the vacancies as a function of the orientation of the magnetic axis was calculated. This calculation is based on the observation that the energy per spin presented in Fig. 4 expresses, in a mean field sense, the reduction in energy (up to an additive constant) associated with the substitution of a Fe^{3+} with an O^{2-} at a B site located at an angle θ to the magnetization axis of the nanoparticle. The effect of the vacancy distribution on the energy may be calculated by simply summing the energy per spin associated with each of the vacancies, and subtracting from the total energy of the equivalent nanoparticle *without*

vacancies. The energy variation as a function the orientation of the magnetization axis of a nanoparticle from the K10 ensemble is shown in Fig. 6 for the $T = 0$ case. The blue patches indicate the preferred location of the magnetization axis. The equivalent calculation for finite T would show a qualitatively similar landscape but with a smaller overall variation in energy due to the more homogenous nature of the average energy per surface spin.

In conclusion, the simulations show the presence of a Néel-like domain wall in the surface magnetization at the magnetic equator separating the radially outward pointing surface spins in the northern magnetic hemisphere from the radially inward pointing surface spins in the southern magnetic hemisphere. Most interesting is the apparent role of the surface vacancies (oxygen sites) in pinning this equatorial domain wall. We close by noting that the energy landscape presented in Fig. 6 not only serves to illustrate the effect of the surface vacancies but also suggests a macrospin model that would be amenable to other approaches (e.g., kinetic Monte Carlo [22–25] or forward flux sampling [26,27]) that could be used to simulate systems of γ-Fe_2O_3 nanoparticles at experimentally relevant cooling rates and field-sweep rates. Such simulations could potentially provide a means to qualitatively probe the effect of the surface anisotropy on experimental $M(T)$ ZFC scans and $M(H)$ hysteresis loops.

[1] C. Altavilla and E. Ciliberto, *Inorganic Nanoparticles: Synthesis, Applications, and Perspectives* (CRC Press, Boca Raton, FL, 2011).

[2] Ò. Iglesias, A. Labarta, and X. Batlle, J. Nanosci. Nanotechnol. **8**, 2761 (2008).

[3] J. Zhang, F. H. B. Lema, H. Shao, K. Sasaki, J. X. Wang, J. Hanson, and R. R. Adzic, J. Phys. Chem. B **109**, 22701 (2005).

[4] K. M. Spiers, D. M. Paganin, and J. D. Cashion, J. Phys.: Condens. Matter. **23**, 176004 (2011).

[5] J. M. D. Coey, Phys. Rev. Lett. **27**, 1140 (1971).

[6] H. Kachkachi and E. Bonet, Phys. Rev. B **73**, 224402 (2006).

[7] R. Yanes, O. Chubykalo-Fesenko, R. F. L. Evans, and R. W. Chantrell, J. Phys. D **43**, 474009 (2010).

[8] R. H. Kodama and A. E. Berkowitz, Phys. Rev. B **59**, 6321 (1999).

[9] J. Mazo-Zuluaga, J. Restrepo, F. Muñoz, and J. Mejia-López, J. Appl. Phys. **105**, 123907 (2009).

[10] F. Vernay, Z. Sabsabi, and H. Kachkachi, Phys. Rev. B **90**, 094416 (2014).

[11] R. H. Kodama, A. E. Berkowitz, E. J. McNiff, Jr., and S. Foner, Phys. Rev. Lett. **77**, 394 (1996).

[12] K. Adebayo, Magnetic nanoparticles, Master's thesis, University of Manitoba, 2009.

[13] D. Kechrakos, K. N. Trohidou, and M. Vasilakaki, J. Magn. Magn. Mater. **316**, e291 (2007).

[14] M. L. Plumer, J. van Lierop, B. W. Southern, and J. P. Whitehead, J. Phys.: Condens. Matter **22**, 296007 (2010).

[15] D. Brinis, A. Laggoun, D. Ledue, and R. Patte, J. Appl. Phys. **115**, 173906 (2014).

[16] M. Woińska, J. Szczytko, A. Majhofer, J. Gosk, K. Dziatkowski, and A. Twardowski, Phys. Rev. B **88**, 144421 (2013).

[17] G. M. da Costa, E. De Grave, and R. Vandenberghe, Hyperfine Interact. **117**, 207 (1998).

[18] R. M. Cornell and U. Schwertmann, *The Iron Oxides: Structure, Properties, Reactions, Occurences and Uses*, 2nd ed. (Wiley-VCH, Weinheim, 2003).

[19] G. Salazar-Alvarez, J. Qin, V. Šepelák, I. Bergmann, M. Vasilakaki, K. N. Trohidou, J. D. Ardisson, W. A. A. Macedo, M. Mikhaylova, M. Muhammed, M. D. Baró, and J. Nogués, J. Am. Chem. Soc. **130**, 13234 (2008).

[20] R. F. L. Evans, W. J. Fan, P. Chureemart, T. A. Ostler, M. O. A. Ellis, and R. W. Chantrell, J. Phys.: Condens. Matter **26**, 103202 (2014).

[21] T. N. Shendruk, R. D. Desautels, B. W. Southern, and J. van Lierop, Nanotechnology **18**, 455704 (2007).

[22] R. W. Chantrell, A. Lyberatos, and E. P. Wohlfarth, J. Phys. F: Met. Phys. **16**, L145 (1986).

[23] Y. Kanai and S. H. Charap, IEEE Trans. Magn. **27**, 4972 (1991).

[24] P.-. Lu and S. H. Charap, J. Appl. Phys. **75**, 5768 (1994).

[25] T. J. Fal, J. I. Mercer, M. D. Leblanc, J. P. Whitehead, M. L. Plumer, and J. van Ek, Phys. Rev. B **87**, 064405 (2013).

[26] R. J. Allen, C. Valeriani, and P. R. ten Wolde, J. Phys.: Condens. Matter **21**, 463102 (2009).

[27] C. Vogler, F. Bruckner, B. Bergmair, T. Huber, D. Suess, and C. Dellago, Phys. Rev. B **88**, 134409 (2013).